Low-Cost Open-Hardware System for Measurements of Antenna Far-Field Characteristics in Non-Anechoic Environments

Jan Olencki
Faculty of Electronics,
Telecommunications and Informatics
Gdansk University of Technology
Gdansk, Poland
jan@olencki.pl

Vorya Waladi
Faculty of Electronics,
Telecommunications and Informatics
Gdansk University of Technology
Gdansk, Poland
vorya.waladi@pg.edu.pl

Adrian Bekasiewicz
Faculty of Electronics,
Telecommunications and Informatics
Gdansk University of Technology
Gdansk, Poland
bekasiewicz@ru.is

Abstract—**Experimental validation belongs to the most important steps in the development of antenna structures. Measurements are normally performed in expensive, dedicated facilities such as anechoic chambers, or open-test sites. A high cost of their construction might not be justified when the main goal of antenna verification boils down to demonstration of the measurement procedure, or rough validation of the simulation models used for the development of the structure. Although solutions for far-field measurement of antennas in non-anechoic environments have been demonstrated in the literature, they utilize expensive equipment. In this work, a low-cost (around 3300 USD), system for experimental validation of antenna prototypes in non-anechoic conditions has been discussed. Its main components include the in-house developed heads and an open-hardware-based vector network analyzer. Performance of the system has been demonstrated using two antenna structures for which radiation patterns have been obtained. Comparisons against measurements performed in the anechoic chamber and using other expensive equipment have also been provided.**

Keywords—**antenna far-field characteristics, non-anechoic measurements, time-gating method, internet of things.**

I. INTRODUCTION

Prototype measurements belong to the most important steps in the development of microwave components. The main goal is to assess performance of structures, as well as to verify electromagnetic (EM) simulation models utilized in the course of the design process. Experimental validation of microwave components such as filters and couplers is relatively straightforward as it boils down to measurements of electrical parameters such as reflection, transmission, or isolation between respective ports [1]. The process is normally performed using vector network analyzers (VNAs). Performance figures of antennas, however, include not only the electrical, but also the field-related responses [2]. The latter include, e.g., radiation patterns, gain, and/or axial ratio of the radiator under test [3]. On the conceptual level, measurements of radiation performance are similar to validation electrical characteristics. The typical setup includes a reference antenna (RA) and the antenna under test (AUT) connected to, e.g., VNA [2-4]. From the measurement perspective, the RA-AUT system is a two port device, where transmission between the antennas (i.e., S_{21}) is realized (in a far-field) through the wireless propagation medium [2], [5]. Consequently, radiation properties are obtained through repetitive measurements of S_{21} as a function of AUT position w.r.t. RA. The latter often remains a static part of the system [2], [3].

Due to the nature of far-field measurements, the fidelity of the extracted AUT radiation characteristics vastly depends on the dynamics of the test environment (here, understood as temporal changes of propagation conditions on the RA-AUT path) [4]. Consequently, for accuracy, the measurements are performed in strictly controlled conditions that ensure electrical shielding of the external EM radiation sources, as well as attenuation of the interference signals [3], [5]. Suitable propagation conditions can be obtained in dedicated facilities that include anechoic chambers, compact range test sites, and others [2-5]. Alternatively, the measurements can be performed in the remote open-air facilities that are characterized by substantially lower levels of background EM radiation than, e.g., urban areas [5-8]. On the other hand, the discussed test environments require expensive and dedicated infrastructure (i.e., chambers, control rooms, high-fidelity positioning and measurement equipment, and others). Consequently their construction might not be justified for budget-constrained applications such as teaching [4]. In the latter case, one might argue that demonstrating and explaining the details of the antenna testing procedure is more important than achieving very high measurement accuracy. Furthermore, provided low-cost of the test system, its damage (e.g., resulting from misuse by students) will not incur high repair costs.

Non-anechoic test sites represent an interesting alternative for the dedicated antenna measurement facilities [7-9]. Their main advantage is relatively low deployment cost, which is due to neglecting the components for shielding of the test environment, or attenuation of stray signals. Instead, non-anechoic measurements are performed at sites that are not tailored for far-field experiments. These include office rooms, or even reverberation enclosures [9], [10]. Limited control (or lack of thereof) over the propagation conditions results in substantial contamination of the AUT-RA signals by the external noise, which renders the measurements useless for drawing any conclusions unless appropriate post-processing is performed [4].

The most popular approaches for correction of the far-field antenna measurements include matrix pencil and time-gating methods (TGM), as well as their derivatives [6-15]. The former class of techniques involves representation of the RA-AUT transmission using a series of functions that correspond to the line-of-sight (LoS) and the reflected signals [16]. Their coefficients find application for

reconstruction of the LoS transmission between the antennas. In TGM, the frequency measurements are converted to time-domain and truncated around the fraction of the impulse response that corresponds to LoS using a tailored window function. The resulting characteristic is then converted back to the frequency spectrum [17], [18]. It is worth noting that TGM proved to be useful for correcting the measurements performed in various non-anechoic test conditions [6], [9], [11].

Regardless of the potential resulting from the applicability of post-processing methods, the cost-related advantages of non-anechoic measurements are neglected in the literature. In [18], the TGM has been utilized to improve the accuracy of far field characteristics obtained in the anechoic chamber, which remains expensive. While validation of antenna performance in test sites contaminated by the external noise has been considered [4], [9], [11], the measurements have been performed using expensive, laboratory-grade VNAs. From this perspective, the problem of cost-efficient measurements of antenna prototypes with reasonable accuracy remains open.

In this work, a low-cost system for measurements of antenna radiation characteristics in non-anechoic environments has been discussed. The system consists of two in-house-developed heads capable of controlling the RA-AUT position in two degrees of freedom, an open-hardware-based VNA that operates in a frequency range of up to 6 GHz [19], as well as control electronics and the software for data acquisition and post-processing. The performance of the discussed setup has been demonstrated using two antenna structures through measurement of the radiation patterns at a set of selected frequency points. Comparisons of the measured characteristics with the ones obtained in noisy environments using expensive VNA, as well as in anechoic chamber have also been provided. For the considered experiments, the average discrepancy between the results obtained using the discussed system and in a controlled environment is around 0.3 dB. At the same time, the cost of the presented setup amounts to 3329 EUR which is negligible compared to the construction cost of professional antenna measurement facilities.

II. MEASUREMENT SYSTEM

A block diagram of the test system for non-anechoic antenna measurements is shown in Fig. 1. It consists of: (i) rotary heads with control electronics, (ii) open-hardware VNA, (iii) radio-frequency (RF) cables, and (iv) control software. The rotary heads have been designed in Autodesk Inventor [20]. Each comprises a steel, in-house machined core that is rotated through a gear with a 1/3.6 ratio driven by a 200-step motor, which ensures angular resolution of up to 0.5°. The core is interconnected with a steel-machined base through a pair of bearings that ensure low-friction rotation. The base contains mounting pins for a standard geodesy tribrach with three-axis precise leveling that is mounted on a tripod. RF connectivity through the core is maintained using a high performance SR1803 rotary joint from Fairview Microwave [21]. The step motor is controlled through a custom driver circuit with an STM8 microcontroller, electrostatic discharge protection, and communication based on a RS-485

standard [22], [23]. Both heads are enclosed in custom housings fabricated using additive technology. Connection to the personal computer (PC) is realized through a standard USB-to-RS-485 adapter. Figure 2 shows a photograph of one of the manufactured heads.

The measurements are performed using LibreVNA—a low-cost, open-hardware, vector network analyzer capable of acquiring a full two-port scattering matrix that represents to the RA-AUT system [19]. The device is utilized as both a source and detector of the signal. It operates within the 100 kHz to 6 GHz range and permits adjustment of frequency bandwidth, as well as resolution according to the considered measurement scenario. It is worth noting that the utilized VNA offers acquisition of up to 4501 frequency points during a single sweep, which exceeds the capabilities of many professional devices [24].

The coaxial cables—Sucoflex, 126 manufactured by Huber+Suhner [25]—are equipped with 3.5 mm adapters. Direct connection to the antennas is realized through the Minibend-16 assemblies [25], which offer a relatively small bending radius, high phase stability and low loss. Positioning of the heads, as well as acquisition of the measurement data are realized using a standard PC and the custom software developed in Python. The communication between PC and VNA is realized over the USB using a standard commands for programmable instruments (SCPI) interface [27].

III. TGM-BASED POST-PROCESSING

Post-processing of the measurements is realized using a time-gating algorithm with automatic calibration of the test site. Here, a brief description of the method and site-calibration algorithm is provided. For more comprehensive discussion see [4], [9], [18].

A. Time-Gating Algorithm

The goal of the process is to perform a correction: $\boldsymbol{R} \rightarrow \boldsymbol{R}_c$, where $\boldsymbol{R} = \boldsymbol{R}(\omega, \boldsymbol{\Phi})$ is a matrix of transmission coefficients (S_{21}) between RA and AUT measured for the given vector of K points $\boldsymbol{\omega} = [\omega_1 \ldots \omega_K]^T$ that represents the sweep around the frequency of interest $f_0 = 0.5 \cdot (\omega_K + \omega_1)$ in a function of P angular positions of AUT $\boldsymbol{\Phi} = [\phi_1 \ldots \phi_P]^T$; $\boldsymbol{R}_c = \boldsymbol{R}_c(f_0, \boldsymbol{\Phi})$ is the corrected far-field response of the AUT for the vector of $\boldsymbol{\Phi}$ angles. Note that $\boldsymbol{R}_c$ can be also used to represent single-direction antenna gain vs. M-point frequency sweep as $\boldsymbol{R}_{cg}(\boldsymbol{f}, \phi) = [R_c(f_1, \phi_p) \ldots R_c(f_M, \phi_p)]^T$, where $\boldsymbol{f} = [f_1 \ldots f_M]^T$ and ϕ_p is the selected angular position of the RA-AUT system.

For the given position ϕ_p, the time-gating algorithm steps can be summarized as follows [4], [9], [11]:

1. Filter the frequency-domain response $\boldsymbol{R}(\omega, \phi_p)$ to attenuate the responses at the edges of the sweep $\boldsymbol{\omega}$;
2. Convert the attenuated response to the N-point time-domain representation $\boldsymbol{T}(t, \phi_p)$;
3. Apply a time-domain window around the part of the impulse response that corresponds to LoS transmission;
4. Convert the modified impulse response back to the N-point frequency-domain and truncate the obtained data to K-points.

The above procedure is repeated for all P angles that represent positions of the AUT w.r.t. the RA. It should be noted that performance of the TGM algorithm is affected by parameters such as bandwidth $B = \omega_K + \omega_1$ around f_0 (which affects resolution of the signal in time-domain as $\partial t = B^{-1}$), but also the number of frequency points K (and hence the frequency resolution $\partial \omega = \omega_2 - \omega_1$), time-domain sweep N, as well as the location and length of the time-gating window [4], [9], [18]. Here, $K = 201$, $N = 2^{\log 2(\lceil K \rceil) + 3}$, and $B \geq c \cdot (3 \cdot D)^{-1}$, where D is the antenna size and c is the speed of light, are selected based on the recommendations from [4]. The parameters of the time-gating window are determined using the test site calibration method described below.

B. Test Site Calibration

The goal of the test site calibration process is adjustment of time-gating window so as to maximize TGM performance in non-anechoic environments. The main assumption behind the method is availability of a so-called calibration antenna (CA), i.e., the structure already characterized in anechoic chamber or using the high-fidelity EM simulations.

The calibration algorithm involves determination of tight window intervals around the impulse response to minimize the effects of noise on the measured antenna performance. Figure 3 illustrates the example window function applied to the time-domain representation of the signal, as well as the effects of adjusting the window intervals on the fidelity of the corrected measurements. As can be seen, optimal intervals represent a narrow valley with steep slopes, which indicates that their appropriate adjustment is crucial for obtaining high-quality measurement results [4].

The calibration process involves measurement of the CA in the non-anechoic test site, followed by optimization of intervals at a set of J frequencies of interest $f_0 = \{f_{0,j}\}_{j=1\ldots J}$. At each frequency $f_{0,j}$, the initial interval bounds are estimated as $t_{j.1}^{(0)} = \min(t_{\text{pos},j})$ and $t_{j.2}^{(0)} = \min([\max(t_{\text{pos},j}), t_{\max,j}])$, where $t_{\text{pos},j} = [t_1 \ldots t_P]^T$ and its components are obtained as [4]:

$$t_p = \arg\max_{t_p \in t}\left(\left| T\left(t, \phi_p\right)\right|\right) \tag{1}$$

whereas $t_{\max,j} = 2 \cdot M(t_{\text{pos},j}) - \min(t_{\text{pos},j})$—with $M(\cdot)$ being the median operation—is used to mitigate the effect of signal reflections on the accuracy of interval estimation [4].

Next, a greedy heuristic method is used to approximate the set of perturbed designs t_{pert} around the $t_{j.1}$, $t_{j.2}$ bounds. In each iteration i, the generated perturbations are evaluated and the best combination of bounds is selected as the optimum for the next step. The designs are evaluated as [4]:

$$\left[t_{j.1}^{(i+1)}\ t_{j.2}^{(i+1)}\right] = \arg\min_{t_{j.1},\ t_{j.2}\in t_{\text{pert}}^{(i)}} U\left(t_{\text{pert}}^{(i)}\right) \tag{2}$$

where U is a scalar objective function of the form [4]:

$$U = \left\| R_{c.i}\left(f_{0.j}, \Phi\right) - R_r\left(f_{0.j}, \Phi\right)\right\|_2 \tag{3}$$
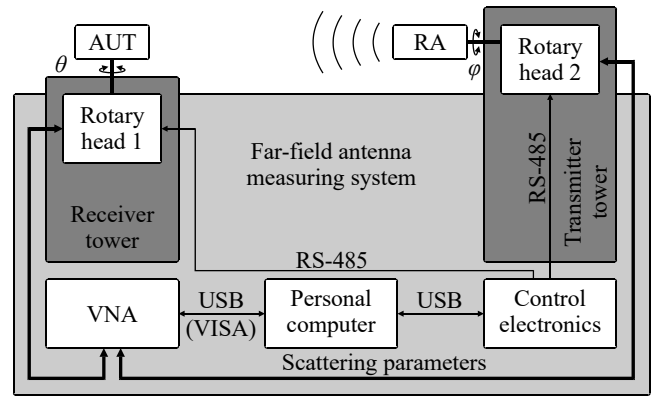

Fig. 1. Block diagram of the open-hardware measurement system.
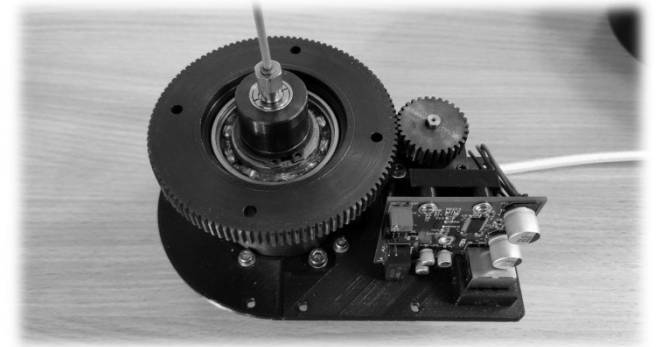

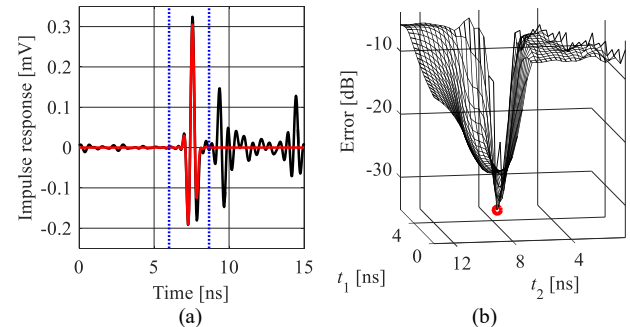Fig. 2. Head of the manufactured positioning system without enclosure.

Fig. 3. Test site calibration: (a) visualization of the impulse response obtained for the CA before (black) and after (red) application of the window function, as well as (b) averaged discrepancy between measurements from the anechoic chamber and unshielded test site as a function of t_1, t_2 intervals.

Here, $R_{c.i}$ represents the corrected response of the CA obtained for $t_{j.1}$, $t_{j.2} \in t_{\text{pert}}^{(i)}$, at the $f_{0.j}$ frequency and R_r denotes the reference response (e.g., obtained in the anechoic chamber, or from EM simulations). The optimization is terminated when the correction performance is the same for two consecutive iterations. The final intervals are obtained as $t_{j.1}^* = t_{j.1}^{(i)}$ and $t_{j.2}^* = t_{j.2}^{(i)}$, respectively.

Upon execution of the algorithm for all j frequency points, the final interval bounds are obtained as $t_1^* = \lfloor <\{t_{j.1}^*\}_{j=1\ldots J}> \rfloor$ and $t_2^* = \lceil <\{t_{j.2}^*\}_{j=1\ldots J}> \rceil$, where $\lfloor \cdot \rfloor$, $\lceil \cdot \rceil$, and $<\cdot>$ denote round down, up to the nearest multiple of ∂t, and average operations. Once the calibration is performed, it is considered valid for the given test site and the antennas characterized by comparable dimensions. For comprehensive discussion on the discussed correction procedure see [4].

IV. RESULTS AND DISCUSSION

In this section, the discussed system for non-anechoic far-field measurements is demonstrated using two broadband antennas: (i) an antipodal Vivaldi structure and (ii) a compact monopole radiator. The considered tests include measurements of the antenna radiation patterns (with 5° resolution) in azimuth plane. Discussion of the results and cost-breakdown of the system are also provided.

The non-anechoic test site used for tests is a 5.7 × 4.5 × 3.1 m³ office room that is not tailored to the far-field measurements, except for installation of the setup discussed in Section II. The line-of-sight between the RA and AUT is around 1.5 m, whereas the distance between AUT to the nearest wall is 1.9 m. The room is full of equipment such as cabinets, desks, or computers that distort the propagated signals. Photograph of the test setup is shown in Fig. 4.

A. Vivaldi Antenna

Figure 5 shows a photograph of the Vivaldi antenna [4]. The radiator is implemented on a Rogers RO4360G2 substrate (ε_r = 6.15, h = 0.81 mm, tanδ = 0.0038). For the considered experiments, the structure is used as both the RA and AUT. The antenna size is roughly 10 cm, which corresponds to B = 1 GHz (see Section III.A) [4].

The first step of the measurement procedure involves calibrating the test site at (arbitrarily selected) 5 GHz frequency. The reference data for the procedure are high-fidelity EM simulations of the radiator. The time-gating bounds obtained using the algorithm of Section III.B are t_1^* = 3 ns, and t_2^* = 9 ns, respectively. Next, the antenna radiation patterns have been measured at 2 GHz, 4 GHz, and 5.5 GHz frequencies and refined using the TGM routine of Section III.A. A comparison of the measured characteristics before and after correction with the responses obtained in the anechoic chamber is shown in Fig. 6. The average discrepancy between the reference and corrected responses—expressed in terms of a root-mean square error (RMSE) averaged over frequency points—is only –22.8 dB, which represents over 6.6 dB improvement w.r.t. the uncorrected radiation patterns.
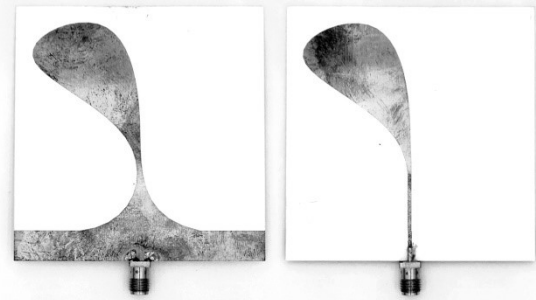

Fig. 5. Vivaldi antenna: photographs of the prototype used for tests of the measurement system [4].
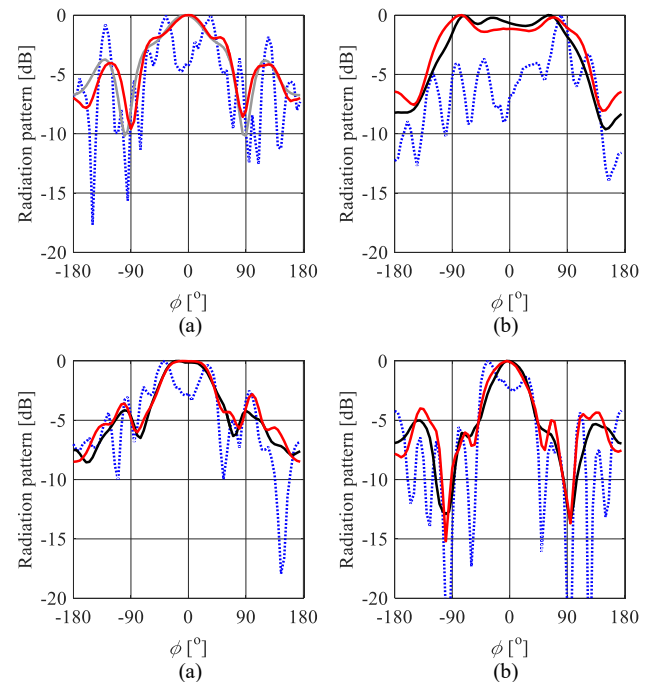

Fig. 6. Radiation patterns of the Vivaldi antenna before (blue) and after (red) post-processing at: (a) calibration frequency of 5 GHz (gray line represents far-field pattern obtained from EM simulations), as well as evaluation frequencies of (b) 3 GHz, (c) 4 GHz, and (d) 5.5 GHz, respectively. Black lines represent measurements from anechoic chamber.

B. Compact Monopole

Our second test case involves measurements of the compact spline monopole antenna shown in Fig. 7 [4]. The structure is implemented on a Rogers RO4003C substrate (ε_r = 3.38, h = 0.76 mm, tanδ = 0.0027). Here, the Vivaldi radiator of Section IV.A is used as RA. The measurement bandwidth for the antenna has been set to B = 2 GHz. It is worth noting that the selected value is narrower than recommended in [4]. Nonetheless, it represents a trade-off between the measurement accuracy and operational bandwidth of the VNA.

The test site has been calibrated at 5 GHz frequency (with respect to radiation patterns obtained from high-fidelity EM simulations) using the method of Section III. The extracted time-gating interval bounds of t_1^* = 4.5 ns, and t_2^* = 5.5 ns, respectively, are narrower than the ones obtained in Section IV.A. In the next step, the antenna radiation patterns have been measured at 3 GHz, 4 GHz, and 5.5 GHz. The obtained results, shown in Fig. 8, indicate that—for the first two frequencies of interest—the

Fig. 4. Photograph of the low-cost open-hardware system for measurement of antenna far-field responses installed in the non-anechoic test site.

resemblance between the corrected responses and the ones from anechoic chamber is high. Slightly worsened results at 5.5 GHz frequency stem from a measurement bandwidth of the VNA, which is insufficient to obtain the responses in the required range (i.e., from 4.5 GHz to 6.5 GHz). Notwithstanding, the improvement of the response w.r.t. uncorrected pattern is still substantial. The average RMSE discrepancy between the reference and refined responses is only –26.1 dB (13.3 dB improvement compared to direct measurements).

C. Discussion

The presented test system has been compared in terms of the accuracy (expressed as averaged difference between EM simulations and measurement responses) against: (i) anechoic chamber, and (ii) version of the non-anechoic setup where the open-hardware VNA is replaced by a laboratory-grade device [24]. For the sake of fair comparison, the test-site calibration settings for measurements performed using open-hardware and professional VNAs remain unchanged. The results gathered in Table I indicate that, for the considered test cases, the performance difference between the results obtained using two different VNAs is small. It results from slight changes in antenna positioning between the tests, as well as the "dynamics" of the environment [4]. At the same time, the open-hardware VNA is almost 90-fold cheaper compared to the professional device. As already indicated, the discrepancy between the characteristics obtained in the chamber and non-anechoic test site is acceptable, and can be considered suitable for applications such as teaching, or low-budget research. On the other hand, low-price of the open-hardware VNA comes at the expense of narrow frequency range (up to 6 GHz) which may be a limiting factor when evaluation of contemporary (e.g., broadband) antenna structures is required.

A cost-breakdown of the discussed system measurements is provided in Table II. It is worth noting that the antenna positioning system (heads, base, and electronics) corresponds to only 21% of the overall cost, whereas the VNA and connectivity equipment amount to 20% and 59%, respectively. High cost of the RF cables is due to their frequency range that vastly exceeds capabilities of the open-hardware VNA, and thus can be easily reduced. Nonetheless, with the overall cost of around 3329 EUR, the presented system is two orders of magnitude cheaper when compared to the laboratory-grade VNA used for tests summarized in Table I. From this perspective, the discussed system is an affordable solution with a range of applications where achieving the laboratory grade precision of measurements is not of primary concern.
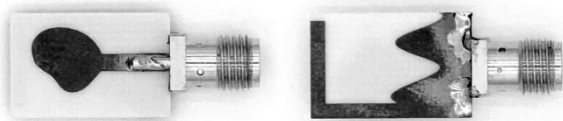

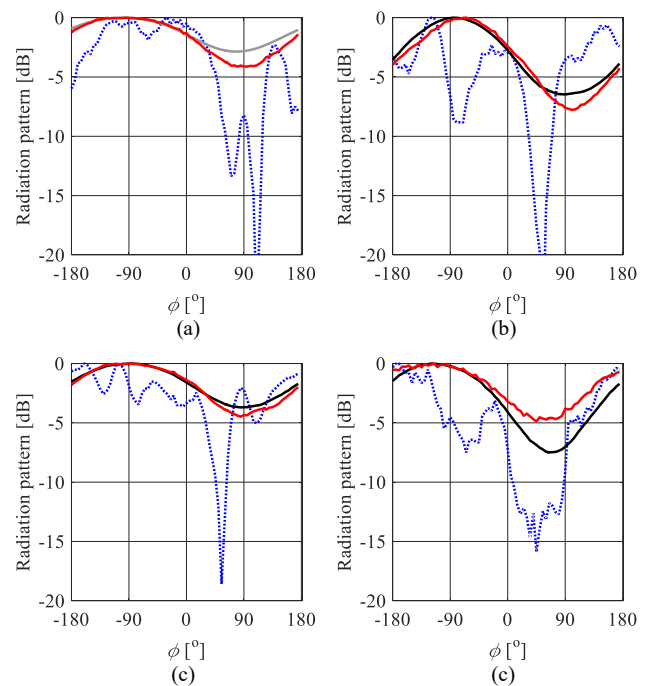Fig. 7. Monopole antenna: photographs of the prototype used for tests of the measurement system [4].

Fig. 8. Radiation patterns of the monopole before (blue) and after (red) correction: (a) calibration at 5 GHz (gray line represents EM-based pattern), as well as evaluation at (b) 3 GHz, (c) 4 GHz, and (d) 5.5 GHz, respectively. Black solid lines represent anechoic chamber measurements.

TABLE I. MEASURED ANTENNA PERFORMANCE VS. EM SIMULATIONS

Setup	Antenna		Average change
	Vivaldi	Monopole	
(i)	1.24 dB	1.70 dB	—
(ii)	1.25 dB	1.78 dB	0.05 dB
This work	0.84 dB	1.50 dB	0.31 dB

TABLE II. MEASUREMENT SYSTEM: COST-BREAKDOWN

Category	Item	Cost [EUR]	Fraction of cost [%]
Heads	Steel and components	137	4.12
	Tools	48	1.44
Base	Tribrachs	104	3.12
	Tripods	237	7.12
Electronics	Components	147	4.42
	PCB manufacturing	22	0.66
	Rotary joints	449	13.5
RF connectivity	Cables	1303	39.1
	Connectors and adapters	216	6.52
Excitation	VNA	666	20.0
Total cost		3329	100.0

V. CONCLUSIONS

In this work, a low-cost system for measurement of antenna far-field characteristics in non-anechoic environments has been discussed. Apart from in-house developed heads that provide two degrees of freedom adjustment of the RA-AUT position, the components of the system include the two-port, open-hardware VNA which operates in a frequency range of up to 6 GHz, but also RF connectivity gear, and the post-processing software. The performance of the discussed system has been demonstrated using the antipodal Vivaldi and compact monopole

antennas. The obtained radiation patterns have been compared against the ones obtained in the anechoic chamber, as well as in the non-anechoic test site yet in the setup with laboratory-grade VNA. For the considered experiments, the average discrepancy between the measurements performed in controlled environment and using the presented system are around 0.31 dB. At the same time, the cost of the discussed setup amounts to only 3329 EUR which makes it suitable, e.g., for applications such as teaching or low-budget research.

Future work will focus on development of low-cost measurement heads that will be suitable for fabrication using additive technologies such as fused deposition modeling or stereolitography. It is expected that utilization of mentioned technologies, substitution of rotary joints with flexible cables, as well as replacement of customized electronics with off-the-shelf components will reduce the cost of the system by a factor of two.

REFERENCES

[1] D.M. Pozar, *Microwave Engineering*, 4th ed., John Wiley & Sons, 2012.

[2] C.A. Balanis, *Antenna theory analysis and design*, 3rd ed., John Wiley & Sons, Hoboken, 2005.

[3] L. Hemming, *Electromagnetic Anechoic Chambers: A fundamental Design and Specification Guide*, IEEE Press, Piscataway, 2002.

[4] A. Bekasiewicz, S. Koziel, and M. Czyz, "Time-gating method with automatic calibration for accurate measurements of electrically small antenna radiation patterns in non-anechoic environments," *Measurement*, vol. 208, art no. 112477, 2023.

[5] G. Evans, *Antenna Measurement Techniques*, Artech House, 1990.

[6] S. Kurokawa, M. Hirose, and K. Komiyama, "Measurement and uncertainty analysis of free-space antenna factors of a log-periodic antenna using time-domain techniques," *IEEE Trans. Instrumentation Meas.*, vol. 58, no. 4, pp. 1120-1125, April 2009.

[7] V. Molina-Lopez, M. Botello-Perez, and I. Garcia-Ruiz, "Validation of the open-area antenna calibration site at CENAM," *IEEE Trans. Instrumentation Meas.*, vol. 58, no. 4, pp. 1126-1134, 2009.

[8] N. Munic, M. Nikolic Stevanovic, A. Djordjevic, and A. Kovacevic, "Evaluation of radiating-source parameters by measurements in Faraday cages and sparse processing," *Measurement*, vol. 104, pp. 105-116, 2017.

[9] A. Soltane, G. Andrieu, E. Perrin, C. Decroze, and A. Reineix, "Antenna radiation pattern measurement in a reverberating enclosure using the time-gating technique," *IEEE Ant. Wireless Prop. Lett.*, vol. 19, no. 1, pp. 183-187, 2020.

[10] V. Fiumara, A. Fusco, G. Iadarola, V. Matta and I. M. Pinto, "Free-space antenna pattern retrieval in nonideal reverberation chambers," *IEEE Trans. EM Comp.*, vol. 58, no. 3, pp. 673-677, 2016.

[11] P. Piasecki and J. Strycharz, "Measurement of an omnidirectional antenna pattern in an anechoic chamber and an office room with and without time domain signal processing," *Signal Proc. Symp.*, pp. 1-4, Debe, Poland, 2015.

[12] G. Leon, S. Loredo, S. Zapatero, and F. Las-Heras, "Radiation pattern retrieval in non-anechoic chambers using the matrix pencil algorithm," *Prog. EM. Res. Lett.*, vol. 9, pp. 119-127, 2009.

[13] Z. Du, J.I. Moon, S.-S. Oh, J. Koh, and T.K. Sarkar, "Generation of free space radiation patterns from non-anechoic measurements using Chebyshev polynomials," *IEEE Trans. Ant. Prop.*, vol. 58, no. 8, pp. 2785-2790, 2010.

[14] D.A. Leatherwood and E.B. Joy, "Plane wave, pattern subtraction, range compensation," *IEEE Trans. Ant. Prop.*, vol. 49, no. 12, pp. 1843-1851, 2001.

[15] B. Fourestie and Z. Altman, "Gabor schemes for analyzing antenna measurements," *IEEE Trans. Ant. Prop.*, vol. 49, pp. 1245-1253, 2001.

[16] B. Fourestie, Z. Altman, J. Wiart, and A. Azoulay, "On the use of the matrix-pencil method to correlate measurements at different test sites," *IEEE Trans. Ant. Prop.*, vol. 47, no. 10, pp. 1569-1573, 1999.

[17] E.N. Clouston, P.A. Langsford, S. Evans, "Measurement of anechoic chamber reflections by time-domain techniques," *IEE Proc.*, vol. 135, no. 2, pp. 93-97, 1988.

[18] S. Loredo, M.R. Pino, F. Las-Heras, and T.K. Sarkar, "Echo identification and cancellation techniques for antenna measurement in non-anechoic test sites," *IEEE Ant. Prop. Mag.*, vol. 46, no. 1, pp. 100-107, 2004.

[19] LibreVNA, an open-hardware vector network analyzer; GitHub project available at: github.com/jankae/LibreVNA

[20] Inventor, Autodesk Inc., One Market, Ste. 400 San Francisco, CA 94105, USA.

[21] Rotary joint SR1803, Fairview Microwave, Inc. 301 Leora Ln., Suite 100, Lewisville, TX 75056, USA.

[22] STM8-Series Microcontroller, STMicroelectronics, 39 Chemin du Champ-des-Filles, Geneve, Switzerland.

[23] RS-485, Telecommunications Industry Association, 1320 North Courthouse Road, Suite 890, Arlington, VA 22201, USA.

[24] MS2038C, Anritsu Corp., 5-1-1 Onna, Atsugi-shi, Kanagawa 243-8555, Japan.

[25] Microwave cable assemblies, Huber+Suhner, Tumbelenstrasse 20, 8330 Pfaffikon ZH, Switzerland.

[26] SCPI, IVI Foundation Corporate Office, Aaron Hall, PO Box 108, Santa Rosa, CA 95402, USA.